Multi-View Imputation and Cross-Attention Network Based on Incomplete Longitudinal and Multi-Modal Data for Alzheimer's Disease Prediction

Meiyan Huang*,   Tao Wang,   Xiumei Chen,   Xiaoling Zhang,   Shuoling Zhou,   Qianjin Feng*

Abstract

Longitudinal variations and complementary information inherent in longitudinal and multi-modal data play an important role in Alzheimer's disease (AD) prediction, particularly in identifying subjects with mild cognitive impairment who are about to have AD. However, longitudinal and multi-modal data may have missing data, which hinders the effective application of these data. Additionally, previous longitudinal studies require existing longitudinal data to achieve prediction, but AD prediction is expected to be conducted at patients' baseline visit (BL) in clinical practice. Thus, we proposed a multi-view imputation and cross-attention network (MCNet) to integrate data imputation and AD prediction in a unified framework and achieve accurate AD prediction. First, a multi-view imputation method combined with adversarial learning, which can handle a wide range of missing data situations and reduce imputation errors, was presented. Second, two cross-attention blocks were introduced to exploit the potential associations in longitudinal and multi-modal data. Finally, a multi-task learning model was built for data imputation, longitudinal classification, and AD prediction tasks. When the model was properly trained, the disease progression information learned from longitudinal data can be leveraged by BL data to improve AD prediction. The proposed method was tested on two independent testing sets and single-model data at BL to verify its effectiveness and flexibility on AD prediction. Results showed that MCNet outperformed several state-of-the-art methods. Moreover, the interpretability of MCNet was presented. Thus, our MCNet is a tool with a great application potential in longitudinal and multi-modal data analysis for AD prediction. Codes are available at `https://github.com/Meiyan88/MCNET`.

1. Introduction

Alzheimer's disease (AD) is characterized by the irreversible impairment of cognitive functions and is one of the most common neurodegenerative diseases in elderly people [1]. Although no effective cure exists for AD, clinical intervention at the early stage may decelerate its progression. Hence, the early prediction of AD's emergence is important for timely treatment to slow down progressive deterioration [2]. As a prodromal stage of AD, mild cognitive impairment (MCI) can be classified into progressive MCI (pMCI) and stable MCI (sMCI) [3, 4]; such classification is denoted as AD prediction and can be used to identify MCI progression and predict AD early [5].

In clinical practice, the amount of longitudinal and multi-modal data is increasing, and has attracted our attention [6]. On the one hand, multi-modal neuroimages, such as magnetic resonance imaging (MRI) and positron emission tomography (PET) images, can provide complementary structural and functional information [7]. Moreover, extensive studies based on multi-modal neuroimages at a single time point have shown reasonable performance in early AD prediction [4]. However, missing data persist in multi-modal data [8], and some useful information may be lost when only modality-complete data are used in AD prediction [9]. Moreover, only a simple concatenation of multi-modal features was used in most existing studies, which may bring redundant information and fail to exploit potential associations among different modalities [10].

On the other hand, AD is a progressive disease, and some early pathological changes, including structural abnormalities within longitudinal variations, can be captured by longitudinal data [11]. Thus, numerous methods have been proposed to use longitudinal data for accurate AD prediction [12, 27]. Nevertheless, the missing data issue remains a common but great challenge in using longitudinal data. It limits the direct usage of most conventional machine learning or deep learning methods. Besides only using modality-complete and longitudinal data to alleviate this problem, some studies first imputed missing data, and then used the complete data to train a model for AD prediction [13, 14]. This decouple two-stage strategy may lead to sub-optimal results, and model performance is heavily influenced by the chosen imputation method [15]. Many techniques can be used for imputing missing values, such as simple forward/backward filling [16], matrix factorization methods based on singular value decomposition [17], statis-

*Corresponding authors

1

tical methods [6], and machine learning methods [11, 18]. Recently, recurrent neural networks (RNN), such as long short-term memory (LSTM) [19] and gated recurrent unit (GRU) networks [20], have been used on data imputation, and advancements have been made. However, modality-complete data at baseline visit (BL) are required in these methods [14]. Many subjects have no available PET images at BL because of various practical issues (e.g., high cost, poor image quality, and others). Moreover, errors exist in the estimated data, which may affect the performance of subsequent tasks. Therefore, further reducing the errors of imputed data is still a problem to be solved. Additionally, obtaining diagnosis results as early as the patients have the imaging scans at BL is desirable in clinical practice. Thus, we still focus on AD prediction with BL data. How to effectively use disease progression information in longitudinal data, whereas only BL data are required as inputs at the model testing phase is also a problem that need to be considered.

To address the aforementioned challenges, an end-to-end multi-task deep learning framework, named multi-view imputation and cross-attention network (MCNet), was proposed to utilize incomplete longitudinal and multi-modal data for AD prediction (i.e., classify subjects into sMCI and pMCI). The proposed method consists of data imputation and diagnostic modules. These two modules share the same multi-modal features extracted from the RNN-based network for multi-task learning, including data imputation, longitudinal classification, and AD prediction tasks. First, in the data imputation module, a novel multi-view imputation strategy with adversarial learning was designed to utilize long-term temporal dependencies to impute MRI/PET data from a longitudinal view and apply the correlations between different modalities to impute the PET data from a multi-modal view. Moreover, incorporating adversarial learning is conducive to increase the realities and reduce the errors of imputed data. Second, the features obtained from the imputation module were fused by two unique feature fusion blocks, named cross-attention blocks, for final AD prediction. Different missing situations exist in incomplete longitudinal and multi-modal data, which leads to differences in importance among the information contained in the features. Therefore, two cross-attention blocks were developed to weigh features and reflect the information's importance. Then, the fused features were used to accomplish longitudinal classification and AD prediction tasks. With the data imputation strategy and cross-attention blocks, the proposed method extracted disease progression information from longitudinal data during training and directly applied the information on BL data to obtain prediction results without feeding longitudinal data at the testing phase. Based on previous reports, no research has combined longitudinal (i.e., long-term temporal dependencies) and multi-modal

correlations to achieve adversarial multi-view imputation at all time points with small errors and integrated classification and prediction tasks in the same framework to achieve joint optimization for AD prediction. In summary, the contributions of this work are as follows:

- Based on incomplete longitudinal and multi-modal data, we integrated data imputation and AD prediction into a unified network and introduced a multi-task learning strategy to achieve joint optimization and improve the prediction performance.

- We designed a multi-view imputation strategy for different modalities and time points to achieve data imputation that can cope with a wide range of missing data situations. Moreover, we incorporated adversarial learning into the imputation strategy to make an imputation data distribution that was close to the real distribution, thereby further reducing imputation errors.

- We proposed cross-attention blocks to fuse multi-modal features at different time points to capture information importance at different time points and modalities, thereby further improving prediction performance.

- We only used data at BL when testing the model's performance (i.e., achieved AD prediction at BL), which is practical in clinical use. Our model can still perform well when only single-modal data (e.g., MRI) are available at BL. Moreover, the proposed method was trained on two datasets provided by the Alzheimer's Disease Neuroimaging Initiative (ADNI) database (i.e., ADNI-1 and ADNI-2) and tested on two external independent datasets (i.e., ADNI-3 and Open Access Series of Imaging Studies-3 [OASIS-3]). Competitive results were achieved using the proposed method, which further demonstrates the well generalized ability of the proposed method.

2. Related Work

2.1. Multi-Modal AD Analysis

Many studies focused on the applications of multi-modal neuroimages, which contained complementary information, for AD prediction [22]. For example, different deep neural networks were first used to learn high-level features from multi-modal data (e.g., PET, MRI, genetic data, and others) at BL. Then, the features learned from the different modalities were concatenated directly for final AD prediction [23]. Zhou *et al.* [10] proposed a three-stage deep feature learning and fusion framework to accomplish multi-scale feature fusion for AD prediction. Better prediction performance was achieved using multi-modal data than single-modal data. However, the direct concatenation of multi-

modal features may fail to take full advantage of the information from different modalities [22, 23]. Zhang *et al.* [24] addressed this problem by developing a deep multi-modal fusion network to fuse the information of MRI and PET hierarchically based on an attention complementary strategy for AD prediction. Moreover, Zu *et al.* [25] utilized multi-kernel learning to combine multi-modal data for AD diagnosis. Although these strategies can be used to effectively combine multi-modal data, their effects on the feature fusion of longitudinal and multi-modal data need further investigation.

In the longitudinal and multi-modal study, associations among different modalities and correlations among different time points should be considered. Inspired by the self-attention mechanism [26], we introduced two cross-attention blocks to exploit the importance of the features extracted from different modalities at different time points and to enhance AD prediction performance.

2.2. Longitudinal AD Analysis

An increasing number of studies attempted to utilize these data for AD-related analysis with the increasing amount of available longitudinal data collected at follow-up time points [5, 11, 12, 27]. Some studies explored the use of traditional machine learning methods. Huang *et al.* [27] proposed a novel temporal group sparsity regression and additive model to identify the associations between longitudinal imaging and genetic data for the detection of potential AD biomarkers. More recently, deep learning methods have shown great potential in AD analysis and have been applied to related classification and regression tasks with promising performance [6, 13, 14, 21, 28, 29]. Among them, RNN-based deep learning methods are often used in longitudinal studies. Nevertheless, conventional RNNs are designed to be used with complete data; incomplete data still present serious problems for the applications of RNN. Some studies tried to alleviate the negative impact of this problem by taking advantage of RNN to deal with variable-length series data for imaging feature extraction and AD prediction but directly ignored the missing data issue [29]. Che *et al.* [13] designed a GRU-based method (GRU-D) to introduce a decay mechanism using information on the interval and location of missing values. Then, they combined decay rates with the incomplete longitudinal data to accomplish classification. Moreover, Ghazi *et al.* [14] proposed a generalized backpropagation through time algorithm for LSTM, and this method can handle missing input and output values. All the missing values of longitudinal data were initialized with zeros. However, these methods do not fundamentally solve the missing data issue.

2.3. Data Imputation

Missing data is a common issue for longitudinal and multi-modal data and may decrease the accuracy of AD prediction. El-Sappagh *et al.* [6] tried to solve this issue by discarding the subjects with serious missing data conditions and using the *k*-nearest neighbor algorithm to impute missing values for remaining subjects. However, this kind of data imputation method is a decouple two-stage methodology, which may lead to sub-optimal results [15]. Therefore, some studies trained a unified model to accomplish data imputation and prediction or classification simultaneously. Nguyen *et al.* [28] used the temporal dependencies of RNN to impute a set of longitudinal data and performed classification in a unified model. However, only temporal associations were considered in this method, and the correlations between different modalities at a time point may be ignored. Jung *et al.* [21] integrated data imputation and longitudinal data classification into a unified framework by utilizing information on the interval between missing values, the location of missing values, and multivariate relations, where the relations of different modalities can be reflected by the multivariate relations and reasonable data imputation, and classification results can be achieved by this method. However, estimation errors of imputation data may accumulate in these unified training methods during the feedforward of the RNN [30].

Generative adversarial network has unparalleled advantages in data generation. Therefore, Ma *et al.* [15] introduced the adversarial learning strategy into the data imputation and classification framework to solve the accumulated errors problem, which can further improve the classification performance. Inspired by this idea, we also introduced an adversarial loss in the proposed method. This study used such a strategy for the first time in AD longitudinal and multi-modal data imputation. Moreover, we designed a novel multi-view imputation method according to the specific situation of missing data to effectively impute missing data and reduce estimation errors.

Moreover, most existing methods still require longitudinal data as inputs in the testing phase [6, 11, 15, 19, 28]. Instead of using longitudinal data in the process of testing, the proposed method tried to learn helpful disease progression information from longitudinal data when training and then used the learned information to improve AD prediction at BL when testing. We hypothesized that even if longitudinal data was limited, the underlying information of disease trajectories can be leveraged by deep learning approaches. When the model was properly trained, the model was able to judge the trend of the disease from BL data through the learned pattern of disease progression and utilized this auxiliary knowledge to enhance AD predictions. Therefore, only multi-modal data at BL or even single modal data at BL were needed at the testing phase in the proposed
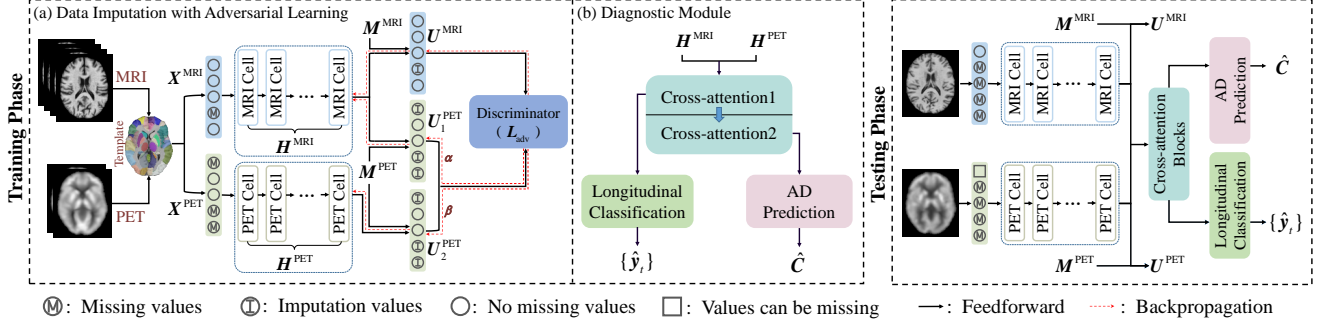
Figure 1. Overview of the proposed framework. (a) Data imputation module with adversarial learning. (b) Diagnostic module for longitudinal classification and AD prediction. In the training phase, MRI and PET data at different time points were trained using modules (a) and (b). In the testing phase, only data at BL were used as inputs, where PET data at BL can be available or missing.

3. Materials

The brain imaging data used in this paper were obtained from the ADNI (https://www.adni.loni.usc.edu/) and OASIS-3 databases (https://www.oasis-brains.org/). A total of 1387 subjects with T1-weighted MRI and fluorodeoxyglucose positron emission tomography (FDG-PET) images in the three ADNI subsets, namely, ADNI-1, ADNI-2, and ADNI-3, were collected in this study. For ADNI-1 and ADNI-2, images at BL and at 6, 12, 24, and 36 months were included when available, whereas only images at BL provided by ADNI-3 were included as the independent testing set. Specifically, subjects that had MRI images at BL and more than two other time points were included, and the available status of PET images was not considered as a criterion for selecting subjects for ADNI-1 and ADNI-2. Moreover, an additional 113 subjects obtained from OASIS-3 were used as another independent testing set. All subjects were categorized into four groups, namely, cognitive normal (CN), sMCI, pMCI, and AD, based on the individual clinical status at BL and future time points. The number of enrolled subjects and more demographic information are shown in Table 1. Subjects with reverse conversion of clinical status were removed. The details of the subject number with different image modalities at different time points are listed in Table 2. Moreover, the preprocessing steps for MRI and PET data were similar with those presented in [9]. Finally, 90-dimensional region-of-interest (ROI) features were separately extracted from the MRI and PET data for each subject.

4. Method

A multi-task learning framework, named MCNet, is proposed for joint data imputation, longitudinal classification, and AD prediction. Fig. 1 presents an overview of the proposed method consisting of two modules. In the first module (Fig. 1 (a)), data imputation was conducted on the MRI

Table 1. Demographic information of ADNI data at BL.

Dataset	Total	Category	Number	Gender (Male/Female)	Age	Mini-mental state examination
ADNI-1	543	CN	165	90/75	75.3 ± 5.2	29.0 ± 1.1
		sMCI	144	91/53	74.6 ± 7.5	27.3 ± 1.6
		pMCI	116	68/48	73.8 ± 6.9	26.8 ± 1.8
		AD	118	60/58	75.1 ± 7.8	23.4 ± 1.9
ADNI-2	758	CN	255	129/126	73.7 ± 5.8	29.1 ± 1.2
		sMCI	286	163/123	71.5 ± 7.5	28.2 ± 1.6
		pMCI	104	57/47	73.4 ± 6.7	27.6 ± 1.9
		AD	113	69/44	74.3 ± 7.8	23.8 ± 2.5
ADNI-3	86	sMCI	73	44/29	75.5 ± 7.6	28.5 ± 1.2
		pMCI	13	8/5	74.0 ± 6.6	26.8 ± 2.8
OASIS-3	143	CN	65	37/28	73.7 ± 8.6	29.2 ± 1.0
		sMCI	48	27/21	74.9 ± 5.6	28.4 ± 1.9
		pMCI	23	19/4	75.6 ± 7.9	27.3 ± 2.3
		AD	7	4/3	76.1 ± 5.6	24.4 ± 1.3

Table 2. Number of available subjects for different modalities at different time points in ADNI-1 and ADNI-2, where M06, M12, M24, and M36 represent 6, 12, 24, and 36 months, respectively.

Dataset	BL	M06	M12	M24	M36
ADNI-1 (MRI/PET)	543/292	534/274	527/267	451/225	284/134
ADNI-2 (MRI/PET)	758/606	534/0	745/111	580/297	396/1

and PET ROI features from the multi-views (i.e., longitudinal and multi-modal views) using a MinimalRNN-based network. Moreover, an adversarial learning block was proposed to reduce imputation errors and increase the realities of the imputed data. Therefore, multi-modal features (hidden features H^{MRI} and H^{PET} in Fig. 1) can be well explored with the imputed data. In the second module (Fig. 1 (b)), two cross-attention blocks were applied to effectively fuse the multi-modal and longitudinal features shared from the data imputation module for longitudinal classification and AD prediction. On the one hand, multi-modal features at each time point were fed into the first cross-attention block to fuse multi-modal information for longitudinal classification. On the other hand, the fused multi-modal features at all time points were fed into the second cross-attention block to exploit potential longitudinal information for AD prediction. The model was trained on all
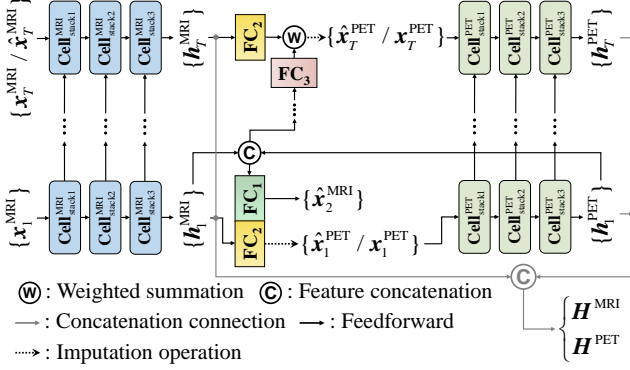
Figure 2. Illustration of data imputation module. The parameters in all time points are shared, i.e., the same memory cells in figure share the same parameters.

available data in the training phase, and only data at BL were used as inputs in the testing phase. The proposed model still performed well when PET data was missing at BL.

4.1. Notations

The ROI features of MRI and PET data can be represented as $\boldsymbol{X} = \{\boldsymbol{X}^S\}_{S=\text{MRI,PET}}$, where S represents the image modality and $\boldsymbol{X}^S = \{\boldsymbol{x}_1^S, ..., \boldsymbol{x}_t^S, ..., \boldsymbol{x}_T^S\} \in \mathbb{R}^{N \times T \times D_1}$. N, T, and D_1 are the subject number, number of time points, and dimension of ROI features, respectively. Missing time points often appear in longitudinal MRI and PET data, and mask vectors $\boldsymbol{M}^S = \{\boldsymbol{m}_1^S, ..., \boldsymbol{m}_t^S, ..., \boldsymbol{m}_T^S\}$ are applied to indicate whether data exist in a time point, where $\boldsymbol{m}_t^S \in \mathbb{R}^{N \times 1}$, and each value in $\boldsymbol{m}_t^S$ is 1 (when $\boldsymbol{x}_t^S$ exists) or 0 (when $\boldsymbol{x}_t^S$ is missing). Moreover, we denote the longitudinal and clinical status labels as $\boldsymbol{Y} = (\{\boldsymbol{y}_t\}_{t=1}^T, \boldsymbol{C})$, where $\boldsymbol{y}_t \in \mathbb{R}^{N \times 1}$ is longitudinal label at t^{th} time point (i.e., if the clinical status is unchanged, $\boldsymbol{y}_t = 0$; otherwise, $\boldsymbol{y}_t = 1$). The longitudinal labels were used in the longitudinal classification task. $\boldsymbol{C} \in \mathbb{R}^{N \times 1}$ indicates the clinical status of a subject. For instance, if the clinical status of a subject is sMCI, then $\boldsymbol{C} = 0$. Otherwise, if it is pMCI, then $\boldsymbol{C} = 1$. Moreover, $\boldsymbol{C}$ is applied to AD prediction.

4.2. Data Imputation with Adversarial Learning

4.2.1 Minimal Recurrent Neural Network

We briefly considered MinimalRNN, which is used as the backbone network of the proposed method. MinimalRNN is a distinctive RNN architecture that adopts the minimum number of operations within RNN without sacrificing performance [31]. Moreover, MinimalRNN can capture longer term dependency, the trainability of which can also be guaranteed.

A single MinimalRNN is a chain structure composed of several memory cells, where each cell corresponds to a time

Table 3. Details of the five cases of missing data, where $\checkmark$ and $\times$ indicate that the data are available and unavailable, respectively.

	Case1	Case2	Case3	Case4	Case5
PET data at BL	$\times$	$\times$	$\times$	$\checkmark$	$\checkmark$
PET data at time point t	$\checkmark$	$\times$	$\times$	$\times$	$\times$
MRI data at time point t	$\checkmark$	$\checkmark$	$\times$	$\checkmark$	$\times$

point. Moreover, all cells share the same parameters. For each cell, the input $\boldsymbol{x}_t^S$ is first fed into a fully connected (FC) network $\Phi(\cdot)$ to achieve a latent representation $\boldsymbol{z}_t^S$. Through this operation, the features are confined to move within this latent space [31]. Given $\boldsymbol{z}_t^S$, the weight of update gate $\boldsymbol{g}_t^S$ can be simply learned with a sigmoid function $\sigma(\cdot)$. Moreover, the update gate $\boldsymbol{g}_t^S$ weighs the contributions of the previous hidden feature $\boldsymbol{h}_{t-1}^S$ and the latent representation $\boldsymbol{z}_t^S$ toward the current hidden feature $\boldsymbol{h}_t^S$. Therefore, the update process can be formulated as:

$$\boldsymbol{z}_t^S = \tanh(\Phi(\boldsymbol{x}_t^S)) = \tanh(\boldsymbol{W}_x \boldsymbol{x}_t^S + \boldsymbol{b}_x^S) \quad (1)$$

$$\boldsymbol{g}_t^S = \sigma(\boldsymbol{W}_h \boldsymbol{h}_{t-1}^S + \boldsymbol{W}_z \boldsymbol{z}_t^S) \quad (2)$$

$$\boldsymbol{h}_t^S = \boldsymbol{g}_t^S \odot \boldsymbol{h}_{t-1}^S + (1 - \boldsymbol{g}_t^S) \odot \boldsymbol{z}_t^S \quad (3)$$

where $\boldsymbol{W}_x$ and $\boldsymbol{b}_x$ denote the parameters of the embedding operation, $\boldsymbol{W}_h$ and $\boldsymbol{W}_z$ denote the parameters related to update gate $\boldsymbol{g}_t^S$, and $\odot$ is the element-wise product. Finally, the hidden features at all time points can be denoted as $\boldsymbol{H}^S = \{\boldsymbol{h}_1^S, ..., \boldsymbol{h}_t^S, ..., \boldsymbol{h}_T^S\}$.

4.2.2 Multi-View Imputation

In this study, longitudinal and multi-modal imaging data were used for accurate AD prediction. However, the missing data issue from longitudinal and multi-modal views is the main limitation when using this type of data. Based on our observations on the ADNI datasets, the cases of missing data can be divided into five types (Table 3). We designed a novel multi-view data imputation method that is different from traditional data imputation methods to impute missing values in different cases and address the complexity of the missing data issue.

Compared with longitudinal MRI images, more serious missing data issue appeared in longitudinal PET images. Therefore, as shown in Fig. 2, we adopted two separate stacked three-layer MinimalRNNs to capture the different longitudinal features of different modalities and then impute data. MinimalRNN cannot perform feedforward when data are unavailable at BL. Therefore, the missing data problem of PET data at BL (i.e., cases 1–3) was considered first. We first imputed the PET data at BL from the multi-modal view using two FC layers with activation function due to the nonlinear relationship between PET and MRI data. We utilized the hidden feature $\boldsymbol{h}_1^{\text{MRI}}$ encoded from the MRI data at BL

to estimate the PET data at BL:

$$\hat{\boldsymbol{x}}_1^{\mathrm{PET}} = \boldsymbol{W}_{\mathrm{cs2}}^{\mathrm{PET}} \tanh(\boldsymbol{W}_{\mathrm{cs1}}^{\mathrm{PET}} \boldsymbol{h}_1^{\mathrm{MRI}} + \boldsymbol{b}_{\mathrm{cs1}}^{\mathrm{PET}}) + \boldsymbol{b}_{\mathrm{cs2}}^{\mathrm{PET}} \quad (4)$$

where $\boldsymbol{W}_{\mathrm{cs1}}^{\mathrm{PET}}$, $\boldsymbol{W}_{\mathrm{cs2}}^{\mathrm{PET}}$, $\boldsymbol{b}_{\mathrm{cs1}}^{\mathrm{PET}}$, and $\boldsymbol{b}_{\mathrm{cs2}}^{\mathrm{PET}}$ are learnable parameters for PET estimation at BL.

For cases 3 and 5, the potential relationship between adjacent time points (i.e., long-term temporal dependencies) was utilized for the imputation of the multi-modal view. Previous temporal contextual information up to time point $t-1$ is contained in the hidden features $\boldsymbol{h}_{t-1}^{\mathrm{MRI}}$ and $\boldsymbol{h}_{t-1}^{\mathrm{PET}}$. Accordingly, the complementary information of different modalities was used for the imputation from the longitudinal view. Specifically, given a time point t, we imputed the missing values through two steps, namely, (a) estimation and (b) imputation. In the first step, the MRI/PET data $\boldsymbol{x}_t^S$ of the current time point can be estimated as:

$$\hat{\boldsymbol{x}}_t^S = \boldsymbol{W}_{\mathrm{long}}^S \mathrm{Concat}(\boldsymbol{h}_{t-1}^{\mathrm{MRI}}, \boldsymbol{h}_{t-1}^{\mathrm{PET}}) + \boldsymbol{b}_{\mathrm{long}}^S \quad (5)$$

where $\boldsymbol{W}_{\mathrm{long}}^S$ and $\boldsymbol{b}_{\mathrm{long}}^S$ are learnable parameters for MRI/PET longitudinal estimation, and $\mathrm{Concat}(\cdot)$ represents feature concatenation. In the second step, $\hat{\boldsymbol{x}}_t^S$ is used if a value is missing, and the new data $\boldsymbol{u}_t^S$ at time point t $(t > 1)$ can be defined as:

$$\boldsymbol{u}_t^S = \boldsymbol{m}_t^S \odot \boldsymbol{x}_t^S + (1 - \boldsymbol{m}_t^S) \odot \hat{\boldsymbol{x}}_t^S \quad (6)$$

We only focused on the imputation from the longitudinal view for MRI data, because in clinical practice, we always have MRI image at a time point. However, the corresponding PET image is missing from the multi-modal view.

For cases 2 and 4, only PET data at current time point t need to be imputed. We adaptively combined the two estimated values obtained from the longitudinal and multi-modal views to calculate the final estimated value at time point t and combine the advantages of multi-view imputation. Specifically, we can take advantage of the hidden features $\boldsymbol{h}_{t-1}^{\mathrm{MRI}}$ and $\boldsymbol{h}_{t-1}^{\mathrm{PET}}$ propagated from the previous $t-1$ time points and utilize the hidden feature $\boldsymbol{h}_t^{\mathrm{MRI}}$ encoded from the MRI data at the same time point t $(t > 1)$:

$$\hat{\boldsymbol{x}}_t^{\mathrm{PET}} = \alpha(\boldsymbol{W}_{\mathrm{cs2}}^{\mathrm{PET}} \tanh(\boldsymbol{W}_{\mathrm{cs1}}^{\mathrm{PET}} \boldsymbol{h}_1^{\mathrm{MRI}} + \boldsymbol{b}_{\mathrm{cs1}}^{\mathrm{PET}}) + \boldsymbol{b}_{\mathrm{cs2}}^{\mathrm{PET}})$$
$$+ \beta(\boldsymbol{W}_{\mathrm{long}}^{\mathrm{PET}} \mathrm{Concat}(\boldsymbol{h}_{t-1}^{\mathrm{MRI}}, \boldsymbol{h}_{t-1}^{\mathrm{PET}}) + \boldsymbol{b}_{\mathrm{long}}^{\mathrm{PET}}) \quad (7)$$

where α and β are learnable weighted coefficients, and $\alpha + \beta = 1$. Similarly, we imputed the longitudinal PET data with mask vectors $\boldsymbol{m}_t^{\mathrm{PET}}$ as listed in (6).

With the imputation steps, the update equation of MinimalRNN can be formulated as:

$$\boldsymbol{h}_t^S = F_{\mathrm{mini}}(\boldsymbol{h}_{t-1}^S, I(\boldsymbol{x}_t^S, \boldsymbol{m}_t^S, \boldsymbol{h}_{t-1}^S), \boldsymbol{\theta}^S) \quad (8)$$

where $\boldsymbol{\theta}^S$ encapsulates the parameters of the MinimalRNN cell, $I(\cdot)$ represents the process of data imputation, and $F_{\mathrm{mini}}(\cdot)$ represents the update function.

Therefore, we can obtain the complete longitudinal MRI and PET data $\boldsymbol{U}^S = \{\boldsymbol{u}_1^S, ..., \boldsymbol{u}_t^S, ..., \boldsymbol{u}_T^S\}$ and corresponding hidden features $\boldsymbol{H}^S$ through the imputation module. Finally, mean absolute error (MAE) was used to measure the estimated loss, which can be defined as:

$$\mathcal{L}_{est} = \sum_{t=1}^{T} \sum_{S}^{\{\mathrm{MRI,PET}\}} (\|\boldsymbol{x}_t^S - \hat{\boldsymbol{x}}_t^S\|_1 \odot \boldsymbol{m}_t^S) \quad (9)$$

4.2.3 Adversarial Learning

Although multi-view estimation was applied to the estimation of longitudinal and multi-modal ROI features, some estimation errors still exist. These errors may be accumulated in the feedforward of MinimalRNN. Thus, an adversarial learning strategy was incorporated into the proposed method to alleviate this dilemma. The adversarial learning block can be defined as a minimax game. Our goal was to learn an imputed data distribution $p_{\mathrm{imp}}(\hat{\boldsymbol{x}})$ that matched the real data distribution $p_{\mathrm{real}}(\boldsymbol{x})$.

Specifically, we added a discriminator consisting of three FC layers so that we can enforce $p_{\mathrm{imp}}(\hat{\boldsymbol{x}})$ close to the $p_{\mathrm{real}}(\boldsymbol{x})$ by fooling the discriminators to reduce the negative impact of missing values. The supervision signal is provided by mask vectors. Thus, the discriminator loss can be defined as follows:

$$\mathcal{L}_{\mathrm{D}} = -[\mathbb{E}_{\boldsymbol{x} \sim p_{\mathrm{real}}(\boldsymbol{x})} \log(\mathrm{Ds}(\boldsymbol{x})) + \mathbb{E}_{\hat{\boldsymbol{x}} \sim p_{\mathrm{imp}}(\hat{\boldsymbol{x}})} \log(1 - \mathrm{Ds}(\hat{\boldsymbol{x}}))] \quad (10)$$

where $\mathrm{Ds}(\cdot)$ denotes the discriminator function, and its output is the estimated mask probability. Therefore, the estimated probability for the real data should be maximized to 1, and the estimated probability for the imputed data should be minimized to 0. Then, we introduced an adversarial loss in the data imputation stage to let MinimalRNN maximize the probability of the discriminator output, which will be backpropagated to further optimize the parameters of the MinimalRNN:

$$\mathcal{L}_{\mathrm{adv}} = \sum_{t=1}^{T} \sum_{S}^{\{\mathrm{MRI,PET}\}} (1 - \boldsymbol{m}_t^S) \odot \log(1 - \mathrm{Ds}(\boldsymbol{u}_t^S)) \quad (11)$$

Thus, our model first updates the discriminators $\mathrm{Ds}(\cdot)$ to distinguish the real data from the imputed data with $\mathcal{L}_{\mathrm{D}}$ and then updates MinimalRNNs with $\mathcal{L}_{\mathrm{adv}}$.

4.3. Diagnostic Module

Our main goal was to perform AD prediction, that is, to classify subjects into sMCI and pMCI at BL using the proposed method. Thus, we designed a diagnostic module to capture the longitudinal and multi-modal associations and then developed two cross-attention blocks to fuse the longitudinal and multi-modal features effectively. Our two modules share the same features extracted by MinimalRNNs.

In this way, we can simply implement a multi-task learning strategy. We accomplished one of the tasks (i.e., data imputation) in the data imputation module. In this module, besides AD prediction, we added another auxiliary task (i.e., longitudinal classification) to exploit predictive representation h_t^S and help the training of the first cross-attention block at each time point, which can contribute to improving the AD prediction performance.

Two cross-attention blocks were developed in our model for feature fusion to effectively combine longitudinal and multi-modal information. In the first cross-attention block, we fused the hidden features from the multi-modal view at each time point through the self-attention mechanism, which was based on a multi-head attention strategy, to explore multi-modal information for longitudinal classification. For each head j, the concatenated hidden features $H_t = \{h_t^{\mathrm{MRI}}, h_t^{\mathrm{PET}}\} \in \mathbb{R}^{N \times 2 \times D_2}$ at a time point t was first translated to three matrices, namely, $Q_t^j \in \mathbb{R}^{N \times 2 \times (D_2/J)}$, $K_t^j \in \mathbb{R}^{N \times 2 \times (D_2/J)}$, and $V_t^j \in \mathbb{R}^{N \times 2 \times (D_2/J)}$, with three projection matrices (i.e., $W_q^j, W_k^j, W_v^j \in \mathbb{R}^{D_2 \times (D_2/J)}$ for all subject), where J is the number of heads, and D_2 is dimension of hidden feautures. Then, the attention matrices A_t^j of different heads can be calculated with Q_t^j, K_t^j, and V_t^j at each head as follows:

$$W_t^j = \mathrm{softmax}(Q_t^j (K_t^j)^T / (\sqrt{D_2/J}) \qquad (12)$$

$$A_t^j = W_t^j V_t^j \qquad (13)$$

where $W_t^j \in \mathbb{R}^{N \times 2 \times 2}$ and $A_t^j \in \mathbb{R}^{N \times 2 \times (D_2/J)}$. Next, all heads were concatenated together on feature dimensions and fed to a FC layer to obtain the residual features, which were used to add to the original features H_t to obtain new features:

$$\tilde{H}_t = W_{\mathrm{att}_1} \mathrm{Concat}(A_t^1 ..., A_t^j, ..., A_t^J) + b_{\mathrm{att}_1} + H_t \quad (14)$$

where $W_{\mathrm{att}_1} \in \mathbb{R}^{D_2 \times D_2}$ and $b_{\mathrm{att}_1} \in \mathbb{R}^{D_2}$ are the parameters of the FC layer for all subjects. We can take advantage of the fused features to classify whether the clinical status changed according to $\tilde{H}_t$ at each time point t:

$$\hat{y}_t = \mathrm{softmax}(W_{\mathrm{cls}} \tilde{H}_t + b_{\mathrm{cls}}) \qquad (15)$$

where W_{cls} and b_{cls} are the learnable parameters for MRI and PET longitudinal classification, and $\mathrm{Softmax}(\cdot)$ denotes activation function. The universal cross-entropy loss for this task is defined as:

$$\mathcal{L}_{\mathrm{cls}} = -\sum_{t=1}^{T} m^{\mathrm{MRI}} \odot (y_t \log(\hat{y}_t) + (1 - y_t) \log(1 - \hat{y}_t))$$
$$(16)$$

where $\hat{y}_t$ is the estimated probability of a clinical status' change at time point t.

Then, AD prediction task was incorporated into the proposed model to achieve accurate AD prediction. Specifically, we concatenated the features in all time points to prevent the loss of contextual information at the early time points, where the concatenated features $H_{\mathrm{pred}} = \{\tilde{H}_1, ..., \tilde{H}_t, ..., \tilde{H}_T\} \in \mathbb{R}^{N \times T \times 2D_2}$ were fed into the second cross-attention block to integrate longitudinal and multi-modal information. Similar to the first cross-attention block, five matrices, namely, $Q_{\mathrm{pred}}^j \in \mathbb{R}^{N \times T \times (2D_2/J)}$, $K_{\mathrm{pred}}^j \in \mathbb{R}^{N \times T \times (2D_2/J)}$, $V_{\mathrm{pred}}^j \in \mathbb{R}^{N \times T \times (2D_2/J)}$, $W_{\mathrm{att}_2} \in \mathbb{R}^{2D_2 \times 2D_2}$, and $b_{\mathrm{att}_2} \in \mathbb{R}^{2D_2}$, were used to calculate the attention matrices $A_{\mathrm{pred}}^j \in \mathbb{R}^{N \times T \times (2D_2/J)}$, corresponding weights $W^j \in \mathbb{R}^{N \times T \times T}$ in each head, and final features $\tilde{H}_{\mathrm{pred}} \in \mathbb{R}^{N \times T \times 2D_2}$ for AD prediction. Moreover, the prediction results were defined as:

$$\hat{C} = \mathrm{softmax}(W_{\mathrm{pred}} \tilde{H}_{\mathrm{pred}} + b_{\mathrm{pred}}) \qquad (17)$$

where W_{pred} and b_{pred} are learnable parameters for AD prediction. The class imbalance in subjects was serious. Thus, focal cross-entropy loss was applied:

$$\mathcal{L}_{\mathrm{pred}} = -\mu(1 - \hat{C})^\gamma \log(\hat{C}) \qquad (18)$$

where μ and γ are set to 0.3 and 2, respectively.

The overall loss function of our proposed method can be defined as follows:

$$\mathcal{L} = \lambda \mathcal{L}_{\mathrm{est}} + \zeta \mathcal{L}_{\mathrm{adv}} + \xi(\mathcal{L}_{\mathrm{cls}} + \mathcal{L}_{\mathrm{pred}}) \qquad (19)$$

where λ, ζ, and ξ hyperparameters. Hence, our model can be trained in an end-to-end manner, and joint optimization for data imputation, longitudinal classification, and AD prediction can be achieved.

Table 4. Details of different testing sets.

Denotation	Included Data	Usage	Subject Number
ADNI-1/2-A	Longtudinal data (incomplete BL data)	Subsection 1) in V.C Section	130 MCI
ADNI-1/2-C	Longtudinal data (complete BL data)	Subsection 2) in V.C Section	81 MCI
ADNI-3-A	BL data (only MRI data)	Subsection 1) in V.C Section	86 MCI
ADNI-3-C	BL data (complete MRI and PET data)	Subsection 2) in V.C Section	86 MCI
OASIS-3-A	BL data (only MRI data)	Subsection 1) in V.C Section	65 MCI
OASIS-3-C	Longtudinal data (complete BL data)	Subsection 2) in V.C Section	65 CN / 6 MCI / 7 AD

5. Experiments

5.1. Experimental Settings

In this study, longitudinal and multi-modal ROI features were used to evaluate the prediction and imputation performances of the proposed method. As described in the *Materials* section, three ADNI subsets, as well as the OASIS-3 database, were enrolled in our experiments. Moreover, the proposed method was implemented using PyTorch, and all experiments were performed on a server with NVIDIA TITAN X (Pascal) GPU.

In the experiments, a hold-out method was used, and all subjects from the ADNI-1 and ADNI-2 datasets were partitioned into 10 non-overlapping subsets with the same proportion of each class. Among which, eight subsets were applied for training, one was utilized for validation, and one was used for testing. For subjects in the training set, data at all available time points were used to train the networks, whereas only data at BL were used to select the hyperparameters and evaluate the networks for subjects in the validation and testing sets. The data partitioning process was repeated five times, and the results of the validation and testing sets were achieved in each process. The final results for the ADNI-1 and ADNI-2 datasets were obtained from the average of five results in the testing set. The subjects in ADNI-3 had FDG-PET scans at BL but had PET scans with other tracers (e.g., Pittsburgh compound B) at subsequent time points, which means that only the PET data at BL were available in ADNI-3 for testing. Different from ADNI-3, OASIS-3 contained a certain amount of longitudinal FDG-PET data. However, in all subjects containing longitudinal MRI and PET data, subjects that belong to the MCI category were lacking. According to the characteristics of different datasets, they were used in the different experiments for performance assessment. See Table 4 for details.

5.2. Implementation Details

The proposed method with five different losses was optimized from three different stages to balance the computational costs and prediction accuracy. Adam optimizer was used in the training process, and a $\ell 2$-regularization was applied to avoid overfitting. The optimized hyperparameters were selected according to the best average value of balanced accuracy (BAC) on the validation set at each step. (a) Data imputation module was first trained separately. The hyperparameters associated with network structure were determined, and the layer number and dimension of hidden features in MinimalRNN were set to 3 and 128, respectively. Moreover, some hyperparameters in (19) were also determined, where λ and ζ were set to 2 and 100, respectively. (b) Diagnostic module was then trained. The parameters of the two cross-attention blocks were optimized in this step, and the number of heads in the blocks was 4. Besides, the data used in the first two steps include all available time points. (c) The two modules were integrated, and end-to-end optimization was achieved using data at BL. In this step, all hyperparameters were finalized: ξ was 10 in (19), learning rate was set to 5×10^{-3}, and weight decay was set to 5×10^{-4}.

Several quantitative metrics were used to evaluate the methods' performance in different tasks. Area under receiver operating characteristic curve (AUC), accuracy (ACC), and BAC were applied for prediction task, and MAE and root mean square error (RMSE) were used for the quantitative evaluation of the imputation task. AUC represents the probability that the predicted positive samples are ranked before the negative samples [32]. It is suitable for handling class imbalance problem in the datasets. Thus, paired t-test (at 95% significance level) was conducted on AUC for statistical significance test in the prediction task. Moreover, paired Wilcoxon signed-rank test [33] (at 95% significance level) was used on MAE as the statistical significance test in the imputation task.

Table 5. Ablation experiments of the proposed method on different datasets for AD prediction. Abbreviations: CB, cross-attention blocks; AL, adversarial learning; DI, data imputation; LC, longitudinal classification.

LC	CB	DI	AL	ADNI-1/2-A			ADNI-3-A			OASIS-3-A		
				ACC	AUC	BAC	ACC	AUC	BAC	ACC	AUC	BAC
×	√	√	√	0.813 ± 0.023	0.832 ± 0.038	0.795 ± 0.024	0.802	0.806	0.789	0.808	0.825	0.772
√	×	√	√	0.815 ± 0.014	0.826 ± 0.030	0.808 ± 0.011	**0.813**	0.819	0.802	0.817	0.820	0.798
√	√	×	√	0.802 ± 0.029	0.818 ± 0.026	0.798 ± 0.027	0.756	0.765	0.761	0.817	0.806	0.786
√	√	√	×	0.812 ± 0.030	0.824 ± 0.024	0.803 ± 0.026	0.791	0.821	0.782	0.798	0.838	**0.801**
√	√	√	√	**0.830 ± 0.019**	**0.842 ± 0.032**	**0.813 ± 0.032**	0.802	**0.849**	**0.820**	**0.827**	**0.857**	0.799

The results of ADNI-1/2-A are reported as mean ± standard deviation.

5.3. Experimental Results and Analysis

5.3.1 Ablation Study

In this section, each of the components in the proposed method was removed separately to investigate its influence on the prediction performance of the proposed method. The results of ablation experiments are shown in Table 5. All ablation experiments were conducted on the ADNI-1 and ADNI-2 testing sets (ADNI-1/2-A), and two other independent testing sets (ADNI-3-A and OASIS-3-A).

First, discarding longitudinal classification brought performance degradation in AD prediction, which indicates that the multi-task learning strategy is useful for AD prediction. Second, the removal of cross-attention blocks led to the direct concatenation of multi-modal features at different time points. The worse result implies that considering the relationships among different modalities at different time points plays an important role in AD prediction. Third, when the data imputation task (i.e., the whole data imputation module) was discarded, all missing data were imputed with mean values, and the corresponding imputation loss listed in (9) was removed. AD prediction performance decreased obviously, which proves the effectiveness of using a unified framework for imputation and prediction. Fourth, AD prediction performance declined when the adversarial learning module was ignored. Moreover, the imputation errors were tested on ADNI-1/2-A after the removal of adversarial learning and compared with the imputation errors produced by the proposed method. The proposed method achieved a 0.049 and 0.063 decrease in MAE and RMSE, respectively, which proves that the adversarial learning module can help further reduce imputation errors

Table 6. Imputation errors and prediction performance of different methods.

Method	ADNI-1/2-C							OASIS-3-C				ADNI-3-C		
	MAE(MRI)	RMSE(MRI)	MAE(PET)	RMSE(PET)	ACC	AUC	BCA	MAE(MRI)	RMSE(MRI)	MAE(PET)	RMSE(PET)	ACC	AUC	BCA
LSTM-Robust	0.686 ± 0.050	1.010 ± 0.065	0.815 ± 0.101	1.049 ± 0.130	0.807 ± 0.021	0.774 ± 0.021	0.774 ± 0.021	0.807	1.027	1.016	1.321	0.760	0.768	0.768
GRU-D	/	/	/	/	0.803 ± 0.038	0.816 ± 0.031	0.795 ± 0.026	/	/	/	/	0.773	0.819	0.775
AJRNN	0.363 ± 0.043	0.511 ± 0.067	0.428 ± 0.036	0.551 ± 0.046	0.831 ± 0.024	0.830 ± 0.016	0.810 ± 0.017	0.398	0.552	0.652	0.746	0.800	0.829	**0.828**
DRM	0.403 ± 0.042	0.574 ± 0.042	0.530 ± 0.015	0.699 ± 0.015	0.821 ± 0.025	0.819 ± 0.030	0.819 ± 0.030	0.588	0.710	0.781	0.891	**0.813**	0.818	0.813
MCNet *	**0.322 ± 0.034**	**0.468 ± 0.062**	**0.415 ± 0.031**	**0.513 ± 0.043**	**0.842 ± 0.012**	**0.860 ± 0.024**	**0.830 ± 0.011**	**0.372**	**0.519**	**0.621**	**0.733**	**0.813**	**0.845**	0.821

The results of ADNI-1/2-C are reported as mean ± standard deviation, and * denotes significant difference with p-value < 0.05

and improve prediction performance.

In summary, the proposed method achieved the best prediction performance, indicating that the proposed components are useful for AD prediction. Moreover, the proposed method achieved AUCs of 0.849 and 0.857 on two independent testing sets under the situation of using only MRI, which demonstrates that imputation from the multimodal view can effectively ensure the prediction performance when only MRI at BL is used. Moreover, the result also proves that our method is flexible in data requirements and can achieve reasonable performance without PET data.

5.3.2 Comparison with Other Methods

Four state-of-the-art AD prediction methods that can also be used to deal with incomplete multi-modal and longitudinal data were applied to compare with the prediction and imputation performances of the proposed method. Moreover, the configurations of different methods are as follows:

- GRU-D [13]: A GRU-based method that designs a decay mechanism using the information on the interval and location of missing values, and combines decay rates with longitudinal data containing missing values to accomplish classification.

- LSTM-Robust [14]: A robust backpropagation is presented through time algorithm by initializing the missing values of inputs to zero and backpropagating zero errors corresponding to the missing values of outputs when training. This algorithm is used in the missing data estimation of longitudinal data, and a two-stage method is used by performing imputation first and then classification.

- Adversarial Joint-learning RNN (AJRNN) [15]: An end-to-end model is trained in an adversarial and joint learning manner, which can directly perform classification with missing values and greatly reduce the error propagation from imputation to classification.

- Deep Recurrent Model (DRM) [21]: A unified framework that applies multivariate and temporal relations inherent in longitudinal and multi-modal data to achieve missing value imputation and model disease progression. The AD prediction result of each subject is obtained using the longitudinal predicted labels acquired from the disease progression task.

Different from the proposed method, complete multimodal data at BL are required for the compared methods. Therefore, the proposed method was also performed on the same subject number (i.e., ADNI-1/2-C, ADNI-3-C, and OASIS-3-C) used in the compared methods for fair comparison. Similar to the proposed method, only multi-modal data at BL were included in the validation and testing sets for the compared methods. For all compared methods, a hold-out method was used, and the hyperparameters were turned carefully according to their corresponding papers to make a fair comparison.

Data imputation may affect the extracted features for final AD prediction. Thus, the imputation errors were quantitatively analyzed on different data imputation methods (i.e., LSTM-Robust, AJRNN, DRM, and the proposed MCNet). During the process of data imputation, all data were estimated regardless of whether the data were missing or not; thus, the data without any missing data can be used as ground truth to evaluate imputation errors. As shown in Table 6, AJRNN and DRM had better imputation results than LSTM-Robust, which indicates that the model based on zero imputation may not be suitable for our data. In comparison with the compared methods, a multi-view imputation combined with adversarial learning strategy was designed in the proposed method to handle missing data issues in different situations. The most important advantage of the proposed method is its ability to deal with missing PET data at BL. Moreover, the inclusion of adversarial learning makes the data distribution close to the real one, thereby further reducing imputation errors and improving the prediction performance. Therefore, the proposed method achieved significantly accurate imputation values compared with the other methods (p-value < 0.05).

The main goal of this study was AD prediction (i.e., pMCI vs. sMCI). The prediction performance of all methods are presented in Table 6, and the following findings were observed. The worst AD prediction results were found in LSTM-Robust. This finding is possibly due to the fact that LSTM-Robust is a two-stage method, in which data imputation and AD prediction are performed separately. Thus, suboptimal results may be obtained using LSTM-Robust. The AD prediction performances of AJRNN and DRM were better than that of GRU-D, which indicates the effectiveness of incorporating data imputation into the AD prediction network in AJRNN and DRM. Additionally, a
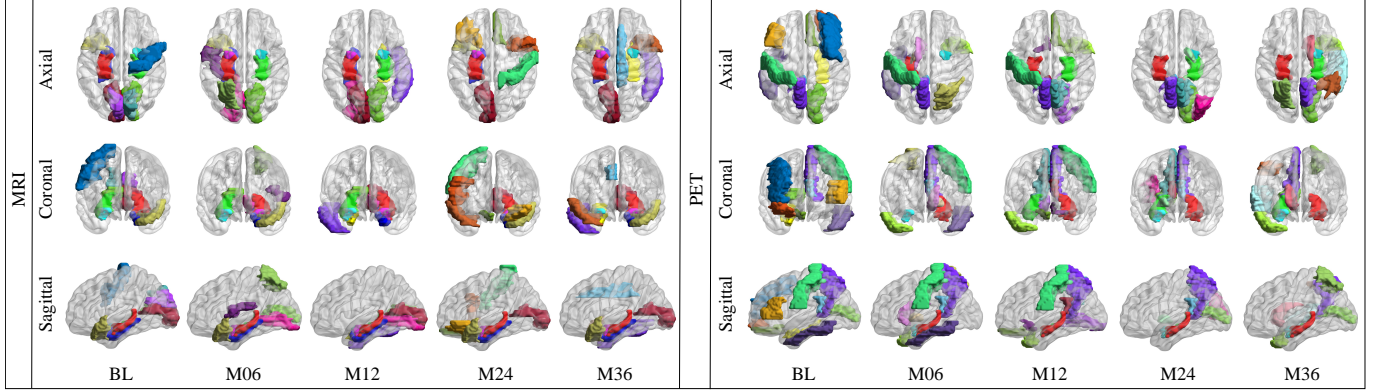
Figure 3. Visualization results of the top-10 ROIs of different modalities at each time point, where M06, M12, M24, and M36 represent 6, 12, 24, and 36 months, respectively.

higher prediction accuracy was achieved using AJRNN than DRM. For DRM, the interval information of missing data was applied to assist in data imputation. However, when only BL data were present, the interval information was lacking, which may lead to poor imputation results and inferior prediction performance in DRM. Moreover, results showed that the proposed method achieved the best performance. A significant difference between the proposed method and the compared methods was found (p-value $<$ 0.05), which implies that the proposed method can be used as a practical and general learning framework for AD prediction on incomplete longitudinal and multi-modal data.

5.3.3 Interpretability of the Proposed Method

The interpretability of the model is crucial for clinical prediction and can help us discover some potential information associated with AD. Therefore, the 10 most discriminative ROIs of different modalities at different time points were illustrated, and their corresponding interpretations were provided.

We introduced a gradient-based computation strategy that computed the contribution of each ROI to longitudinal classification at each time point to locate the most discriminative ROIs [29]. Therefore, based on the contribution values, we screened out the top-10 ROIs of different modalities at different time points. Specifically, for the rth ROI of modality S at the tth time point $\boldsymbol{X}_t^S(r) \in \mathbb{R}^{N \times 1 \times 1}$, the derivatives of the predicted probability $\hat{y}_t$ of the subjects with AD with regard to $\boldsymbol{X}_t^S(r)$ was obtained from the longitudinal classification task, and the absolute value of the derivative among all subjects was averaged as the contribution. The visualization results of the top-10 ROIs of different modalities at each time point are shown in Fig. 3. For MRI, the hippocampus, parahippocampal gyrus, and amygdala, which are highly correlated with memory, were detected at each time point. Higher contribution values

were achieved at 6 and 12 months than at other time points. Moreover, the volume atrophy of these three ROIs is associated with healthy aging and different stages of AD [34]. On the contrary, the parahippocampal gyrus and amygdala were detected at the first two time points, and the hippocampus was detected at the last four time points for PET. Besides, the temporal pole, which is linked to visual cognition, was also detected at most time points in MRI instead of PET. The posterior cingulate gyrus is an important area detected by PET, and the remarkable metabolism reduction in the region is associated with memory impairment, which is a feature of early AD [36]. Furthermore, the precuneus, which is associated with a high level of cognitive function [37], was explored by PET data at most time points. Moreover, the contributions of the detected ROIs varied across different time points and are also worthy of further study.

6. Conclusion

In this study, we proposed an end-to-end multi-task deep learning framework for AD prediction. A multi-view imputation method combined with adversarial learning was developed for incomplete longitudinal and multi-modal data to handle missing data. Moreover, cross-attention blocks were introduced to explore crucial information of different modalities at different time points, which can contribute to the achievement of accurate AD prediction. The proposed method was trained on two ADNI datasets with 1301 subjects. Moreover, two independent testing sets were applied to further evaluate the generalization ability of the proposed method. Based on the experiments, the proposed method achieved high accuracy in missing data imputation and AD prediction and performed well when only MRI data were available at BL. To our best knowledge, no research has combined longitudinal and multi-modal correlations to achieve multi-view adversarial imputation at different time points with small errors, performed AD classification and prediction in the same framework for the joint optimization

of AD prediction, and achieved satisfying AD prediction results using only single-modal data at BL during testing. Therefore, the proposed method may be a crucial tool for AD prediction, diagnosis, and monitoring.

Several issues should be addressed in future research. First, although 1530 subjects were included for training in this study, the number of subjects is still insufficient to fully exploit the potential of deep learning. Moreover, a limited sample size may lead to the overfitting of the model. In the future, more samples will be collected through collaboration with clinicians instead of using publicly available datasets. Second, our model was built based on the ROI features extracted from neuroimages, which resulted in the loss of location information. Therefore, the location information of ROIs need to be introduced in future work. Finally, only PET and MRI data were included in our study. Increasing neuroimaging modalities, such as functional MRI and diffusion tensor imaging, are proven to be effective for AD diagnosis. Hence, an interesting topic for study is the efficient integration of information from other modalities into our framework.

References

[1] J. Gaugler *et al.* "2019 Alzheimer's disease facts and figures," *Alzheimer's & Dementia*, vol. 15, no. 3, pp. 321-387, 2019.

[2] Z. Ning, Q. Xiao, Q. Feng, W. Chen, and Y. Zhang, "Relation-Induced multimodal Shared Representation Learning for Alzheimer's Disease Diagnosis," *IEEE Trans. Med. Imaging*, vol. 40, no. 6, pp. 1632-1645, 2021.

[3] Y. Chen, and Y. Xia, "Iterative sparse and deep learning for accurate diagnosis of Alzheimer's disease," *Pattern Recognit.*, vol. 116, 2021.

[4] W. Zhu, L. Sun, J. Huang, L. Han, and D. Zhang, "Dual Attention Multi-Instance Deep Learning for Alzheimer's Disease Diagnosis With Structural MRI,," *IEEE Trans. Med. Imaging*, vol. 40, no. 9, pp. 2354-2366, 2021.

[5] M. Huang, W. Yang, Q. Feng, W. Chen, and N. Alzheimer's Dis, "Longitudinal measurement and hierarchical classification framework for the prediction of Alzheimer's disease," *Sci. Rep.*, vol. 7, no. 1, pp. 1-13, 2017.

[6] S. El-Sappagh, T. Abuhmed, S. M. R. Islam, and K. S. Kwak, "Multimodal multitask deep learning model for Alzheimer's disease progression detection based on time series data," *Neurocomputing*, vol. 412, pp. 197-215, 2020.

[7] L. K. Ferreira and G. F. Busatto, "Neuroimaging in Alzheimer's disease: current role in clinical practice and potential future applications," *Clinics*, vol. 66, pp. 19-24, 2011.

[8] Y. Pan, Y. Chen, D. Shen, and Y. Xia, "Collaborative Image Synthesis and Disease Diagnosis for Classification of Neurodegenerative Disorders with Incomplete multimodal Neuroimages," *Med. Image Comput. Comput. Assist. Interv (MICCAI)*, 2021, pp. 480-489.

[9] X. Chen, T. Wang, H. Lai, X. Zhang, Q. Feng, and M. Huang, "Structure-constrained combination-based nonlinear association analysis between incomplete multimodal imaging and genetic data for biomarker detection of neurodegenerative diseases," *Med. Image Anal.*, vol. 78, pp. 102419, 2022.

[10] T. Zhou, K. H. Thung, X. Zhu, and D. Shen, "Effective feature learning and fusion of multimodality data using stage-wise deep neural network for dementia diagnosis," *Hum. Brain Mapp.*, vol. 40, no. 3, pp. 1001-1016, 2019.

[11] J. Zhang *et al.*, "Multi-Resemblance Multi-Target Low-Rank Coding for Prediction of Cognitive Decline With Longitudinal Brain Images," *IEEE Trans. Med. Imaging*, vol. 40, no. 8, pp. 2030-2041, 2021.

[12] L. Brand, K. Nichols, H. Wang, L. Shen, H. Huang, and N. Alzheimer's Dis, "Joint multimodal Longitudinal Regression and Classification for Alzheimer's Disease Prediction," *IEEE Trans. Med. Imaging*, vol. 39, no. 6, pp. 1845-1855, 2020.

[13] Z. Che, S. Purushotham, K. Cho, D. Sontag, and Y. Liu, "Recurrent neural networks for multivariate time series with missing values," *Sci. Rep.*, vol. 8, no. 1, pp. 1-12, 2018.

[14] M. M. Ghazi *et al.*, 'Training recurrent neural networks robust to incomplete data: application to Alzheimer's disease progression modeling," *Med. Image Anal.*, vol. 53, pp. 39-46, 2019.

[15] Q. Ma, S. Li, and G. W. Cottrell, "Adversarial joint-learning recurrent neural network for incomplete time series classification," *IEEE Trans. Pattern Anal. Mach. Intell.*, 2020.

[16] Z. C. Lipton, D. C. Kale, and R. Wetzel, "Modeling missing data in clinical time series with rnns," *Machine Learning for Healthcare*, vol. 56, 2016.

[17] J. Cai, E. J. Candès, and Z. Shen, "A singular value thresholding algorithm for matrix completion," *SIAM Journal on optimization*, vol. 20, no. 4, pp. 1956-1982, 2010.

[18] J. Yoon, W. R. Zame, and M. van der Schaar, "Estimating missing data in temporal data streams using multidirectional recurrent neural networks," *IEEE Trans. Biomed. Eng.*, vol. 66, no. 5, pp. 1477-1490, 2018.

[19] S. Hochreiter and J. Schmidhuber, "Long short-term memory," *Neural Comput.*, vol. 9, no. 8, pp. 1735-1780, 1997.

[20] K. Cho *et al.*, "Learning phrase representations using RNN encoder-decoder for statistical machine translation," *arXiv preprint arXiv:1406.1078*, 2014.

[21] W. Jung, E. Jun, H. I. Suk, and N. Alzheimer's Dis, "Deep recurrent model for individualized prediction of Alzheimer's disease progression," *NeuroImage*, vol. 237, p. 118143, 2021.

[22] J. Shi, X. Zheng, Y. Li, Q. Zhang, and Y. Shi, "Multimodal neuroimaging feature learning with multimodal stacked deep polynomial networks for diagnosis of Alzheimer's disease," *IEEE J. Biomed. Health. Inf.*, vol. 22, no. 1, pp. 173-183, 2017.

[23] J. Venugopalan, L. Tong, H. R. Hassanzadeh, and M. D. Wang, "Multimodal deep learning models for early detection of Alzheimer's disease stage," *Sci. Rep.*, vol. 11, no. 1, pp. 1-13, 2021.

[24] T. Zhang and M. Shi, "multimodal neuroimaging feature fusion for diagnosis of Alzheimer's disease," *J. Neurosci. Methods*, vol. 341, p. 108795, 2020.

[25] C. Zu, Y. Wang, L. Zhou, L. Wang and D. Zhang, "multimodality feature selection with adaptive similarity learning for classification of Alzheimer's disease," *Proc. 9th IEEE Int. Symp. Biomed. Imag. (ISBI)*, 2018, pp. 1542-1545.

[26] A. Vaswani *et al.*, "Attention is all you need," in *Proc. Adv. Neural Inf. Process. Syst. (NIPS)*, 2017, pp. 5998–6008.

[27] M. Huang, X. Chen, Y. Yu, H. Lai, and Q. Feng, "Imaging Genetics Study Based on a Temporal Group Sparse Regression and Additive Model for Biomarker Detection of Alzheimer's Disease," *IEEE Trans. Med. Imaging*, vol. 40, no. 5, pp. 1461-1473, 2021.

[28] M. Nguyen, T. He, L. J. An, D. C. Alexander, J. Feng, B. T. T. Yeo, and N. Alzheimer's Dis, "Predicting Alzheimer's disease progression using deep recurrent neural networks," *NeuroImage*, vol. 222, p. 117203, 2020.

[29] M. Huang *et al.*, "Deep-gated recurrent unit and diet network-based genome-wide association analysis for detecting the biomarkers of Alzheimer's disease," *Med. Image Anal.*, vol. 73, p. 102189, 2021.

[30] S. Bengio, O. Vinyals, N. Jaitly, and N. Shazeer, "Scheduled sampling for sequence prediction with recurrent neural networks," in *Proc. Adv. Neural Inf. Process. Syst. (NIPS)*, 2015, pp. 1171–1179.

[31] M. Chen, "Minimalrnn: Toward more interpretable and trainable recurrent neural networks," *arXiv preprint arXiv:1711.06788*, 2017.

[32] J. Huang, C. X. Ling, "Using AUC and accuracy in evaluating learning algorithms," *IEEE Trans. Knowl. Data Eng.*, vol. 17, no. 3, pp. 299-310, 2005.

[33] F. Wilcoxon, "Individual comparisons by ranking methods, " in *Breakthroughs in statistics*: Springer, 1992, pp. 196-202.

[34] S. J. Teipel, *et al.*, "Comprehensive dissection of the medial temporal lobe in AD: measurement of hippocampus, amygdala, entorhinal, perirhinal and parahippocampal cortices using MRI," *J. Neurol.*, vol. 253, no. 6, pp. 794-800, 2006.

[35] B. Herlin, V. Navarro, and C. Dupont, "The temporal pole: From anatomy to function—A literature appraisal," *J. Chem. Neuroanat.*, vol. 113, pp. 101925, 2021.

[36] S. Minoshima, B. Giordani, S. Berent, K. A. Frey, N. L. Foster, and D. E. Kuhl, "Metabolic reduction in the posterior cingulate cortex in very early Alzheimer's disease," *Annals of Neurology: Official Journal of the American Neurological Association and the Child Neurology Society*, vol. 42, no. 1, pp. 85-94, 1997.

[37] A. E. Cavanna and M. R. Trimble, "The precuneus: a review of its functional anatomy and behavioural correlates," *Brain*, vol. 129, no. 3, pp. 564-583, 2006.